CrossMark

Original Research

# Biocompatible hydrophilic brushite coatings on AZX310 and AM50 alloys for orthopaedic implants

Y. Sasikumar[1] · A. Madhan Kumar[2] · R. Suresh Babu[1] · Mohammad Mizanur Rahman[2] · Leandro M. Samyn[1] · A. L. F. de Barros[1]

## Abstract

Dicalcium phosphate dihydrate (DCPD) brushite coating with flake like crystal structure for the protection of AZX310 and AM50 magnesium (Mg) alloys was prepared through chemical deposition treatment. Chemical deposition treatment was employed using $Ca(NO_3)_2 \cdot 4H_2O$ and $KH_2PO_4$ along with subsequent heat treatment. The morphological results revealed that the brushite coating with dense and uniform structures was successfully deposited on the surface of AZX310 and AM50 alloys. The X-ray diffraction (XRD) patterns and Attenuated total reflectance infrared (ATR-IR) spectrum also revealed the confirmation of DCPD layer formation. Hydrophilic nature of the DCPD coatings was confirmed by Contact angle (CA) measurements. Moreover, electrochemical immersion and *in vitro* studies were evaluated to measure the corrosion performance and biocompatibility performance. The deposition of DCPD coating for HTI AM50 enables a tenfold increase in the corrosion resistance compared with AZX310. Hence the ability to offer such significant improvement in corrosion resistance for HTI AM50 was coupled with more bioactive nature of the DCPD coating is a viable approach for the development of Mg-based degradable implant materials.
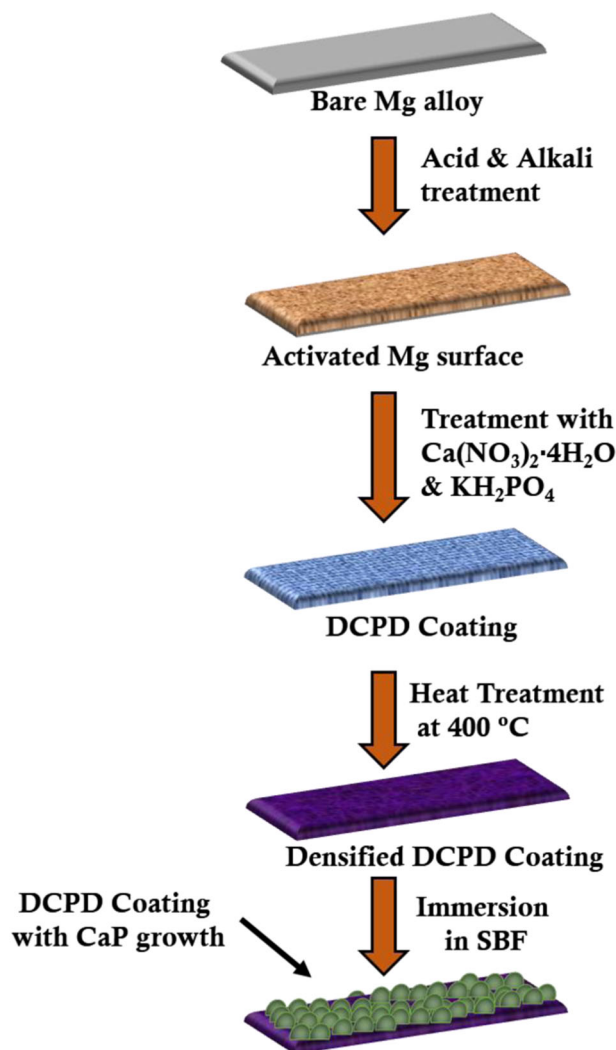
✉ Y. Sasikumar
sasikumar.phd@gmail.com

✉ A. Madhan Kumar
madhankumar@kfupm.edu.sa

1   Laboratory of Experimental and Applied Physics, Centro Federal de Educação Tecnológica Celso Suckow da Fonseca, Av. Maracanã Campus 229, Rio de Janeiro 20271-110, Brazil

2   Center of Research Excellence in Corrosion, Research Institute, King Fahd University of Petroleum and Minerals, Dhahran 31261, Saudi Arabia

**Graphical Abstract**



Bare Mg alloy

Acid & Alkali treatment

Activated Mg surface

Treatment with $Ca(NO_3)_2 \cdot 4H_2O$ & $KH_2PO_4$

DCPD Coating

Heat Treatment at 400 °C

Densified DCPD Coating

DCPD Coating with CaP growth

Immersion in SBF

# 1 Introduction

Magnesium (Mg) alloys acts as biodegradable materials and paid much attention towards the replacement of conventional temporary implants. Mg and its alloys are mainly used for prostheses, particularly for the joint replacements on the manufacturing of orthopaedic implant materials owing to its good biocompatibility and excellent corrosion resistance [1–5]. On comparison to the other materials like ceramics, polymers and other metal implants, Mg alloys plays a major role with excellent biodegradation properties of good mechanical properties with attractive biocompatibility [1, 4, 6] and are very closer to the natural bone with its density and elastic modulus [7, 8]. However, its low corrosion resistance is considered to be one of the main limitations for its clinical usage. Higher rate of osteolysis followed by loosening of the

implant materials takes place due to their lack of bone bonding ability. Abrupt loss with mechanical integrity may occur because of the rapid degradation of implants and the tissues were sufficiently healed to the loosening of the implant on connection with the surrounding tissues [9]. Various possibilities exists to tailor and monitor the corrosion rate with the usage of an suitable surface treatment on Mg alloys which can match the better requirement on the healing of the tissues to provide an adequate and mechanically supported during the implantation at its initial period with a faster degradation rate before the completion of the healing time [10].

Various coatings techniques and surface-modification methods are generally employed for the Mg alloys to improve and enhance its bone bonding ability [11–23]. Protective biocompatible coatings like hydroxyapatite are the most coating material which is preferentially used. Hydroxyapatite (HA) is considered to be one of the main components of bone due to the stable formation of a

crystalline phase with the available calcium phosphate compounds. HA and the other related calcium phosphate compounds like dicalcium phosphate dihydrate (DCPD), β-tricalcium phosphate (β-TCP) are considered to be other preferential coating materials. An expectation of HA coatings on Mg alloys with suitably ideal for scaffolds of artificial bone and bone fixation devices in the biomedical field is an essential requirement. HA is the most preferentially used biomaterial because of its excellent bioactivity with good biocompatibility and almost its chemical structure similar and resemblance to the human natural bone which can accelerate bone concrescence [11].

Surface modification with biocompatible HA coating can improve the implant-tissue interaction on Mg alloys at the requirement of its healing period will control its degradation rate. Various methods of research work on HA coatings on Mg alloys were available which includes biomimetic techniques [12, 13], chemical deposition [14, 15] and electro deposition [16–18]. Methods like plasma spraying, pulsed melting using laser, physical and chemical vapor deposition failed to form proper suitable coating over the surface of Mg alloys due to its poor heat resistance and low melting point [19–25]. Recently, several research studies on Mg alloys have been reported on chemical treatment which includes alkali, acid, conversion and deposition treatments [26]. Chemical surface treatment is considered to be a suitable technique with cost effective is employed for the reduction of corrosion rate on Mg alloys which is very essential for the improvement of biomedical implants. Among the chemical surface treatment, the deposition methods which include the chemical coatings will improve with an excellent bioactive surface coatings on Mg alloys with good corrosion resistance were investigated by various researchers [27–35].

The main objective of this present research work is to obtain the biocompatibility of surface treated AZX310 and AM50 alloys and its electrochemical behavior in SBF solution. The surface treated AZX310 and AM50 alloys was examined using surface characterization techniques such as scanning electron microscopy (SEM) coupled with energy dispersive analysis (SEM-EDS), atomic force microscopy (AFM), X-ray diffractometer (XRD) and attenuated total reflectance infrared spectroscopy (ATR-IR). Contact angle (CA) measurements were also evaluated for the hydrophilicity of the DCPD coating on AZX310 and AM50 alloys.

# 2 Experimental procedure

## 2.1 Materials

AZX310 and AM50 alloys with dimensions of $1 \times 1$ cm$^2$ were used as the test specimens in this work and the Mg alloys composition were given in Table 1.

Table 1 Chemical compositions of AZX310 and AM50 alloys in (wt %)

| Alloys | Main Alloying elements (wt%) | | | | | | |
|---|---|---|---|---|---|---|---|
| | Al | Zn | Mn | Cu | Ca | Ni | Mg |
| AZX310 | 3.20 | 1.32 | 0.18 | 0.08 | 0.31 | 0.09 | Bal. |
| AM50 | 6.20 | – | 0.18 | 0.44 | – | – | Bal. |

## 2.2 Surface treatment of specimens

AZX310 and AM50 specimens were polished with SiC-coated abrasive papers until 2500 grit for the uniform surface roughness and cleaned using acetone with an ultrasonic cleaner for 20 min. Further, the polished specimens are cleaned and rinsed with distilled water and allowed to dry. Then the specimens were chemically washed and cleaned with the HCl:H$_2$O mixture at the ratio of 1:4 (in volume) maintained at 60 °C for 2 min for the removal of oxide layer formation over the specimen's surface. Ultrasonic cleaning was carried out for 20 min with distilled water and dried. Pre-treatment with NaOH was performed with the specimens by soaking with 40 mL of aqueous solution of 1 M NaOH at 60 °C in an oven for 24 h. Further it is thoroughly cleaned and washed well with the distilled water and dried.

## 2.3 Chemical deposition treatment

Chemical deposition treatment was performed in 40 mL of aqueous solution with 0.1 M Ca(NO$_3$)$_2$·4H$_2$O and 0.05 M KH$_2$PO$_4$ by soaking the specimens at 80 °C for 2 h. Further the treated specimens are rinsed and cleaned with distilled water and allowed to dry. The dried specimens were carefully taken and subjected to the heat treatment with 400 °C for 1 h in an air-tight furnace. Further it is allowed to cool until room temperature inside the furnace. The thickness of the DCPD coatings was measured by a coating thickness gauge (Elcometer Instruments, Germany) and the error in the thickness measurements was less than 5%. The average thickness of DCPD coatings was found to be about 14–15.25 μm. The schematic representation of the DCPD coating with the CaP growth is shown in Fig.1.

## 2.4 In vitro bioactive evaluation and degradation behavior

To assess the hydroxyapatite (HA) or CaP growth formation through immersion tests, in vitro bioactive evaluation was performed for the surface treated AZX310 and AM50 alloys in simulated body fluid (SBF) solution for 168 h maintained at 37 °C with pH 7.4. The simulated body fluid solution was prepared based upon the procedure followed by Kokubo and Takadama [36] and used as the electrolyte for all the
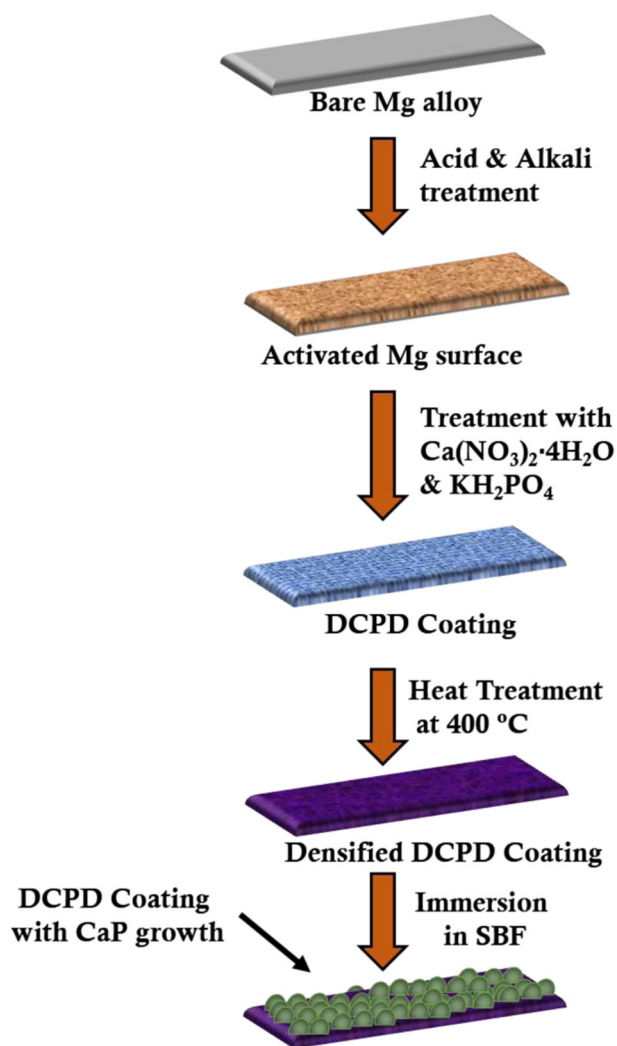
**Fig. 1** Schematic representation of DCPD coating formation with CaP growth

**Table 2** Chemical composition of simulated body fluid (SBF) solution

| S.No. | Reagents used | Grams in 1000 mL |
|---|---|---|
| 1 | NaCl | 8.035 |
| 2 | $NaHCO_3$ | 0.355 |
| 3 | KCl | 0.225 |
| 4 | $K_2HPO_4.3H_2O$ | 0.231 |
| 5 | $MgCl_2.H_2O$ | 0.311 |
| 6 | 1 M HCl | 40 ml |
| 7 | $CaCl_2$ | 0.292 |
| 8 | $Na_2SO_4$ | 0.072 |
| 9 | $((CH_2OH)_3CNH_2)$ | 6.118 |
| 10 | 1 M HCl | Appropriate amount for adjusting the pH 7.4 |

*in vitro* experiments. The chemical composition of simulated body fluid (SBF) solution is presented in Table 2. The SBF solution was replenished to maintain the ionic concentration of the solution for every 24 h during *in vitro* assessment. Electrochemical measurements like potentiodynamic polarization (PDP) and electrochemical impedance spectroscopy (EIS) were carried out for the surface treated AZX310 and AM50 alloys to evaluate the biodegradability behavior in SBF solution. Further, the specimens were taken out from the SBF after the immersion period and thoroughly rinsed and washed with distilled water and allowed to dry. Finally the dried specimens were taken carefully to obtain for further characterization studies.

## 2.5 Surface analysis

Surface morphological behavior was examined using SEM (JEOL, JSM-6360). The surface chemical and elemental analysis was evaluated using energy dispersive X-ray spectroscopy (EDS). The topographical surface was analysed through AFM (Agilent 5500 AFM, USA) instrument. The acquired AFM images were detected with non-contact mode of Au coated silicon cantilevers with a resonance frequency of 26 kHz with a spring constant of 1.6 N/m under air environment. Hydrophilic coating surfaces were measured with Contact angle goniometry interfaced with an attension optical goniometer of well-equipped image-capture software with an introduction of 2 μL liquid drop. The images of drops were processed by the image analysis system, which calculated contact angles from the shapes of the drops with an accuracy of 0.1°.To obtain reliable contact angle data, the water contact angles were measured for five times at different positions and mean of it was selected as final value with a standard error of about ±5°. The phase compositional analysis of was performed using X-ray diffraction (XRD, RINT2500) of an scattering angle of $20° \le 2\theta \le 80°$ at a $2\theta$ step of 0.02° was used. The possible chemical bonds formed in the specimens were characterized by an IR spectrometer (Thermo scientific, with universal ATR attachment, range 500–4000 $cm^{-1}$).

## 2.6 Corrosion analysis

*In vitro* tests were conducted for the surface treated AZX310 and AM50 alloys after 168 h of immersion in SBF to evaluate its corrosion resistance. Electrochemical corrosion experiments were performed using IVIUM Potentiostat/Galvanostat using with an electrochemical cell assembly of three-electrode setup. AZX310 and AM50 alloys acts as the working electrode (WE), saturated calomel electrode (SCE) acts as the reference electrode (RE) and the platinum foil serve as the counter electrode (CE). The surface of the specimens with 1 $cm^2$ was used as the exposed area. To attain for a stable value of open circuit potential (OCP), a stabilization period of 30 min was allowed

**Fig. 2** SEM images of AZX310 **a** UT, **b** HT, **c** HTI and AM50, **d** UT, **e** HT, **f** HTI
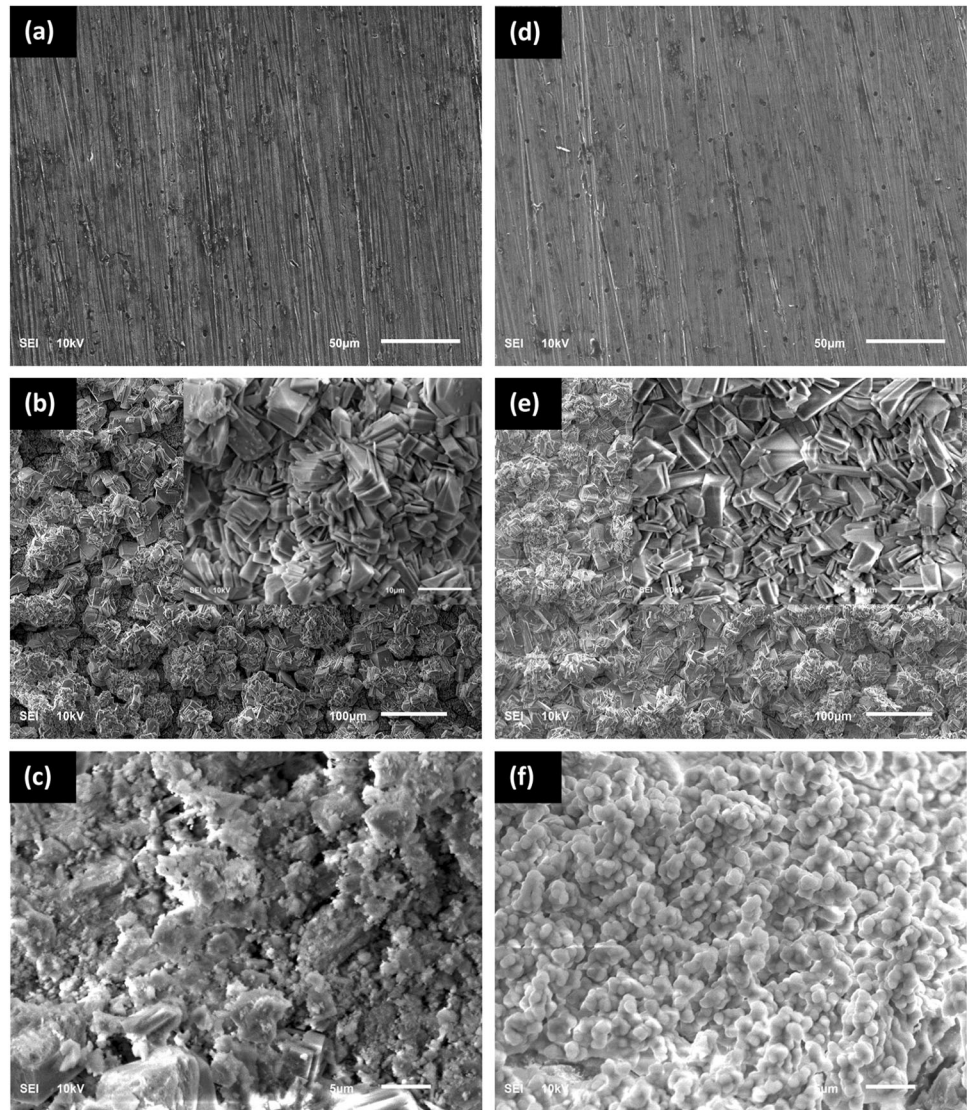


sufficiently before the commencement of all the electrochemical measurements. Potentiodynamic polarization (PDP) was obtained at the potential in the tafel region of $\pm 250$ mV with OCP. The scan rate applied was $1$ mVs$^{-1}$. Electrochemical impedance spectroscopy (EIS) was measured in the frequency range from $10^5$ to $10^{-1}$ Hz at $10$ mV amplitude voltage of peak-to-peak with the AC signal obtained at OCP. To verify for the repeatability and to get the reliable results, all the measurements were tested for triplicate.

# 3 Results

## 3.1 Surface characterisation

The surface morphologies and its elemental compositional analysis were examined using SEM-EDS analysis. The morphological features of SEM micrographs for Untreated (UT), DCPD coating with heat treatment (HT) and DCPD coating with heat treatment after $168$ h of immersion in SBF (HTI) for AZX310 and AM50 alloys were presented in Fig. 2. EDS spectrum obtained for AZX310 and AM50 alloys are presented in Fig. 3. The spectrum represents the coating with various elements of O, Ca, P, Cl, C, Na and Mg.

Topographical AFM images were acquired for UT, HT, HTI AZX310 and AM50 alloys are represented in Fig. 4. Contact angle (CA) values were measured to evaluate the surface hydrophilicity of UT, HT, HTI AZX310 and AM50 alloys and the obtained images were represented in Fig. 5. Contact angle measurements were made by dropping $2$ µL of water drops over the uncoated (UT) and coated (HT, HTI) surfaces at room temperature.

**Fig. 3** EDS images of AZX310
**a** HT, **b** HTI and AM50, **c** HT, **d**
HTI
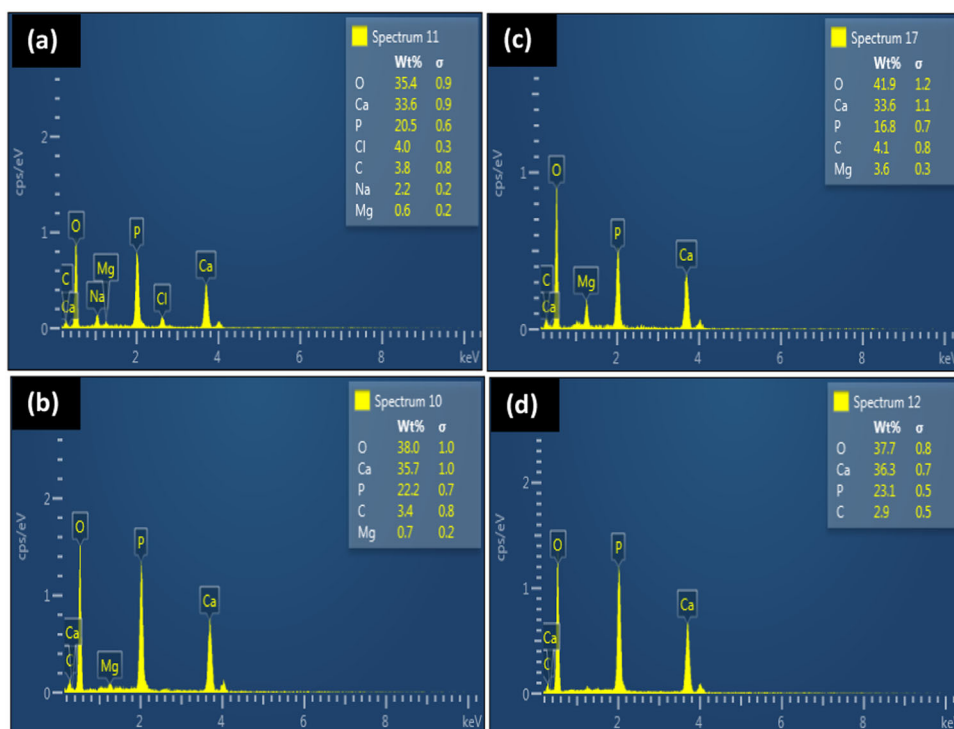


## 3.2 Structural characterisation

XRD spectrum obtained for UT, HT, HTI AZX310 and AM50 alloys are shown in Fig. 6. XRD patterns exhibited the peaks at 2θ values of 26.8°, 29.5°, 30.8°, 31.2°, 32.6°, 34.6°, 37°, 48.2°, 58°, 63.5°, 69° and 73° corresponding to the planes (002), (141), (110), (221), (100), (002), (101), (102), (110), (103), (201) and (004) are in accordance with card data (JCPDS 11-293, JCPDS 20–0669, JCPDS-70-1433). ATR-IR spectroscopy is used to detect the vibrational modes and its corresponding functional groups to detect the growth formation over the surface of the materials. The ATR-IR spectra for UT, HT, HTI AZX310 and AM50 alloys are depicted in Fig. 7.

## 3.3 Electrochemical analysis

Electrochemical corrosion experiments were examined to evaluate the corrosion performance of DCPD coatings on AZX310 and AM50 alloys. The polarization plots obtained for UT, HT, HTI AZX310 and AM50 alloys are shown in Fig. 8. The Tafel polarization curves were recorded during the electrochemical measurements and the various electrochemical parameters viz., corrosion current density ($i_{corr}$), corrosion potential ($E_{corr}$) and the corrosion rate values from the polarization curves were calculated which are presented in Table 3.

Electrochemical impedance spectroscopy (EIS) was analysed to evaluate the passive film/electrolyte interface changes over the Mg surfaces. EIS will also provide the qualitative information about the corrosion properties and its function of the system. EIS measurements were examined for the UT, HT, HTI AZX310 alloy in SBF solution and the corresponding impedance response behavior plots were shown in Fig. 9. The impedance response behavior for the UT, HT, HTI AM50 alloy in SBF solution is shown in Fig. 10.

## 4 Discussion

### 4.1 Surface characterisation

The UT AZX310 (Fig. 2a) and AM50 (Fig. 2d) surfaces represent a unidirectional groove formation with smooth surface texture due to the mechanical grinding. The HT AZX310 (Fig. 2b) and AM50 (Fig. 2e) surfaces exhibited a uniform flake-like crystal structure of DCPD (CaP flakes) and a rectangular shape of CaP flakes (at higher magnifications) with different size in dimensions over the entire surface of the specimens [37, 38]. Meanwhile, the HTI surfaces exhibited different morphological behavior after the immersion in SBF solution. The surface of HTI AZX310 (Fig. 2c) revealed the presence of cluster of white particles over the surface which is evinced as the CaP or apatite (from EDS analysis). On the other hand, the surface of HTI AM50 (Fig. 2f) exhibited isolated globules of uniform shape of spherical white particles coverage over the
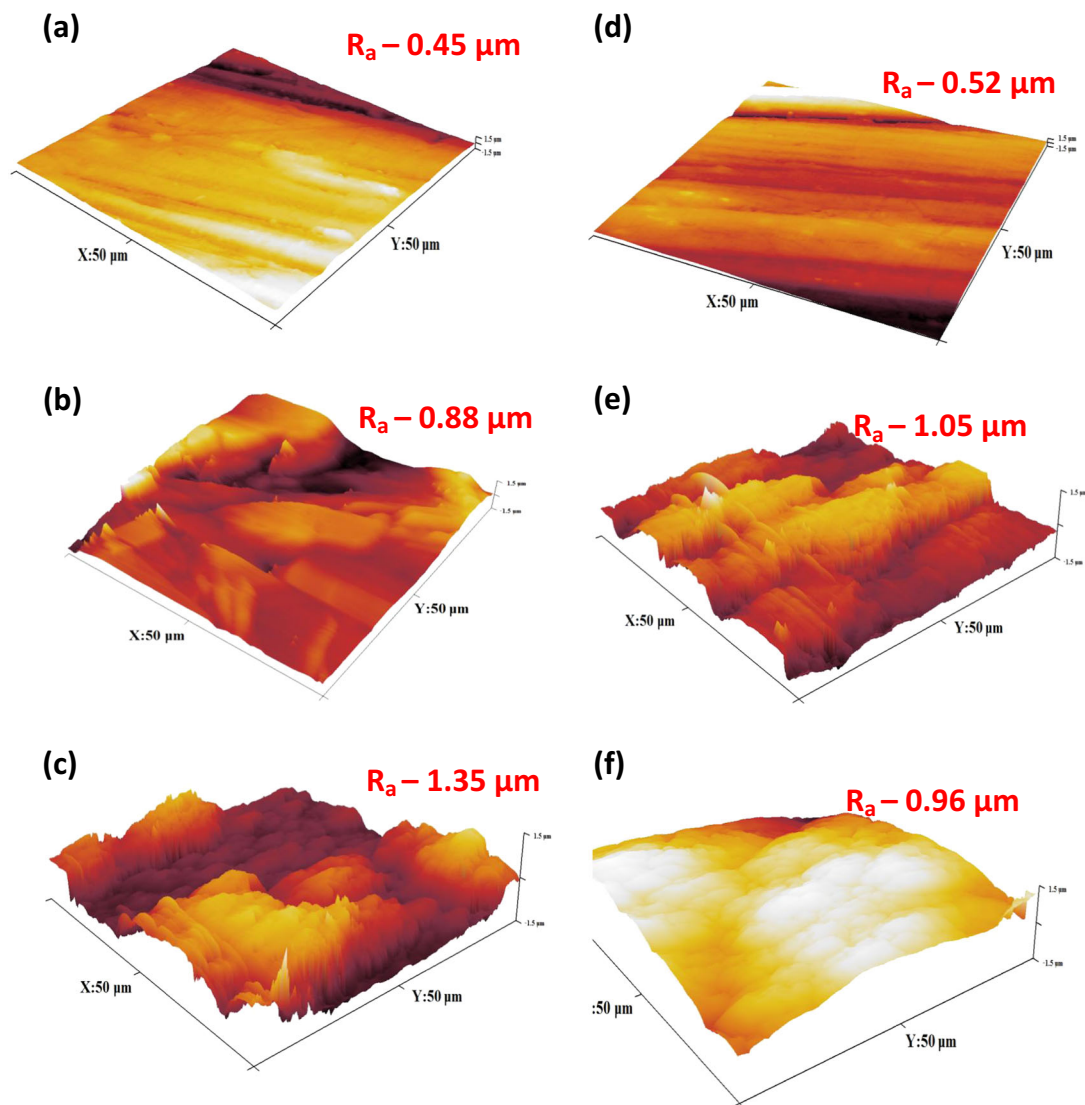
**Fig. 4** AFM images of AZX310 **a** UT, **b** HT, **c** HTI and AM50, **d** UT, **e** HT, **f** HTI

entire surface. The bioactivity of the apatite or CaP was mainly depends upon its elemental compositional analysis.

EDS spectrum obtained after the immersion in SBF for HTI AZX310 (Fig. 3b), and HTI AM50 (Fig. 3d) can be observed that the $Mg^{2+}$, $Na^+$ ions substituted the $Ca^{2+}$ position, meanwhile $CO_3^{2-}$ substituted the $PO_4^{3-}$ or $OH^-$ in biological apatite, similar to the composition or the natural bone mineral. The CaP ratio was found to be 0.82 and the DCPD treated with immersion in SBF was found to be 1.58. However, the theoretical value of HA was found to be 1.67. This represents that the both obtained values were lower than HA. Hence, the DCPD coating was found to be Ca-deficient HA (CDHA) [39]. The Ca/P ratio lies between 1.33 and 1.55 is in accordance with Dorozhkin [40] have analysed the surfaces to induce the formation of new bone *in vivo* were to be more conducive.

The topographic image obtained for UT AZX310 (Fig. 4a) and UT AM50 (Fig. 4d) surfaces reveal a smooth uniform surface texture due to the mechanical polishing. Meanwhile, the HT AZX310 (Fig. 4b) and HT AM50 (Fig. 4e) surfaces exhibited a non-uniform uneven surface with the formation of pores in depth with a roughness value in the range of microscale after the deposition of DCPD coating. The arithmetic of the average roughness ($R_a$) values obtained for UT, HT, HTI AZX310 and AM50 alloys are given in Table 4. The depth of pores and the roughness is slightly reduced for HT AM50 than HT AZX310 due to the uneven surfaces with the formation of DCPD coating. It can be also identified that the HTI surfaces showed the increase in the roughness values obtained for AZX310 (Fig. 4c) and the roughness is highly reduced for HTI AM50 (Fig. 4f) with more surface protection than AZX310 due to the

**Fig. 5** Photographs of water contact angles on the surface of AZX310 and AM50 alloys
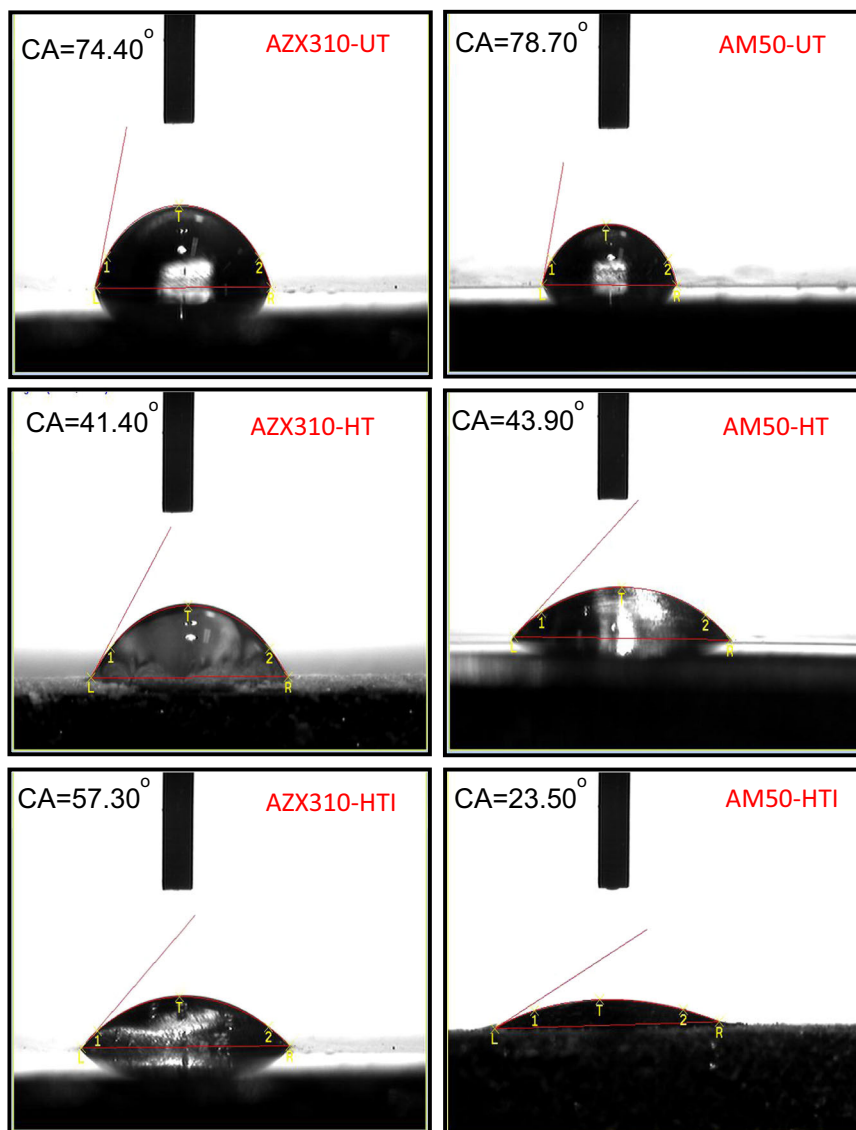


prolonged immersion in SBF has acquire more of the CaP deposition over the HTI AM50 surface [41].

It can be identified that the obtained contact angle (CA) values represent the formation of hydrophilicity surfaces on AZX310 and AM50 alloys. As can be seen that the CA values observed for UT AZX310 and AM50 alloys were 74.40°, 78.70° respectively. Meanwhile for the DCPD coated surfaces (HT AZX310 and AM50 alloys), the water CA values were reduced to 41.40°, 43.90° which represents that the enhancement of hydrophilicity was increased with the presence of more hydrophilic groups formed after the surface treatment on AZX310 and AM50 alloys. Moreover, it can obviously observe that DCPD coating after immersion in SBF for HTI AZX310 surface showed increase in the CA value of 57.30°. However, it can be identified that the HTI AM50 surface has a CA value decreased to 23.50° after DCPD coating on immersion in SBF solution [42].

## 4.2 Structural characterization

High intense peaks were identified for untreated Mg specimens. The XRD peaks exhibited the CaP coating consists mainly of crystalline formation of di-calcium phosphate dihydrate (DCPD, $CaHPO_4 \cdot 2H_2O$) or Brushite (JCPDS 11-293) with Mg, Mg $(OH)_2$ and MgO phase formation on the specimens. No observation for other calcium and phosphate peaks in the spectrum. A new thick layer of brushite formation over the specimens can be observed and hence, the intensity of the diffraction peaks was decreased for HT and HTI specimens. There is also, no enough magnesium peaks observed which may be due to the thick DCPD layer formation for HT and HTI specimens [37–39]. This DCPD coating has the ability to adsorb more of Ca and P ions from the SBF solution during the immersion in SBF, to cause the thick layer
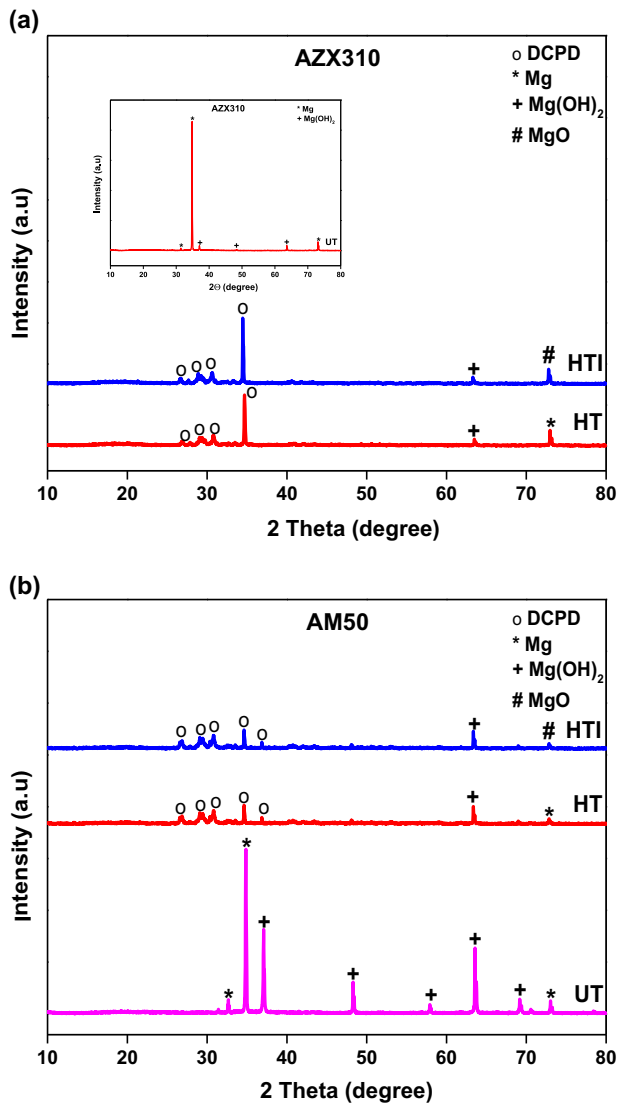
Fig. 6 XRD spectrum of **a** AZX310 and **b** AM50 alloys



Fig. 7 ATR-IR spectrum of **a** AZX310 and **b** AM50 alloys

formation and will induce the nucleation of the CaP growth over the specimens.

The crystallite size of the DCPD coatings from the XRD peaks were calculated using Scherer's equation [43] as follows.

$$D_{hkl} = \frac{k\lambda}{\beta \cos\theta} \qquad (1)$$

where $D_{hkl}$ denotes the crystallite's average diameter, $k$ represents the constant (shape factor 0.89), $\lambda$ is the wavelength of the X-rays (0.154056 nm), $\beta$ is the difference in the width of the half-maximum of the XRD peaks for the pure diffraction profile in radians, $\theta$ is the diffraction angle. The crystallite size values were calculated and the obtained values were in the range from 40 to 80 nm [43].

The spectral bands detected between 2350 and 2340 cm$^{-1}$ represents the DCPD formation [38]. The absorption
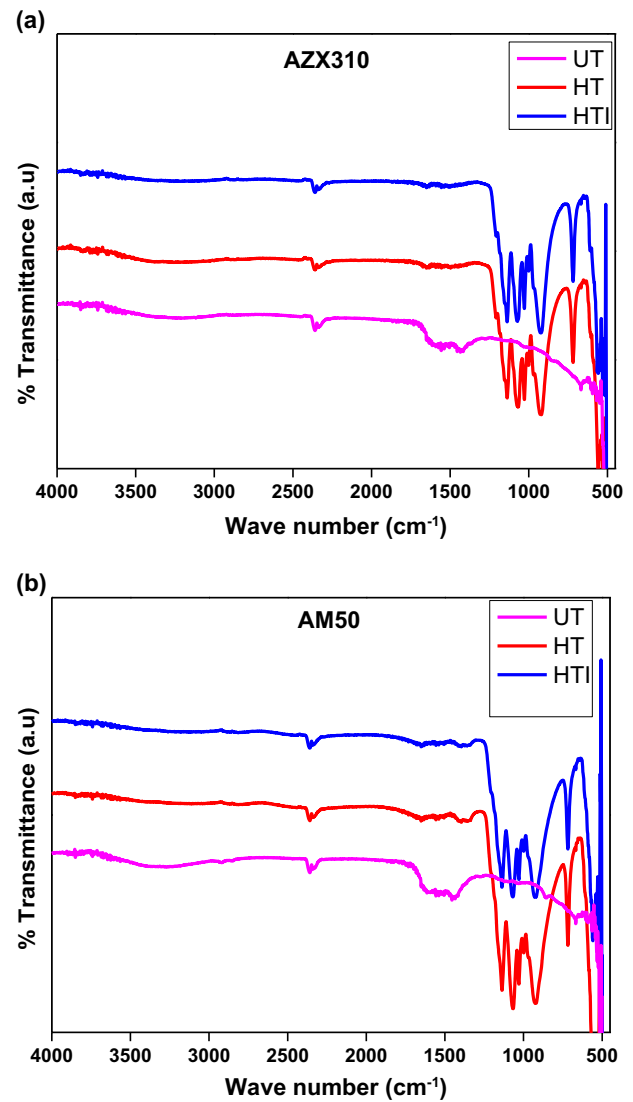
bands observed in the range from 1650 to 1600 cm$^{-1}$ correspond to the bending vibrations of water adsorption. The spectral absorption bands detected between 1480 and 1400 cm$^{-1}$ corresponds to C-O of the CO$_3$ group. A strong $\nu_3$ PO$_4^{3-}$ vibration bands, associated with the internal modes of PO$_4^{3-}$ represents P-O asymmetric stretching vibrations observed at 1142, 1072, 1022, 576 and 513 cm$^{-1}$. The absorption bands around 920–900 cm$^{-1}$ were due to P-OH stretching mode of vibration. The spectral absorption peaks detected at 724 and 713 cm$^{-1}$ is due to the H$_2$O liberation. The bands at 650–600 cm$^{-1}$ belong to triply ($\upsilon_4$) and doubly ($\upsilon_2$) degenerated bending modes of phosphate's O-P-O bonds [43, 44]. The ATR-IR spectrum further confirms the DCPD (Brushite) formation for AZX310 and AM50 alloys which is in accordance with the XRD and SEM-EDS analysis.
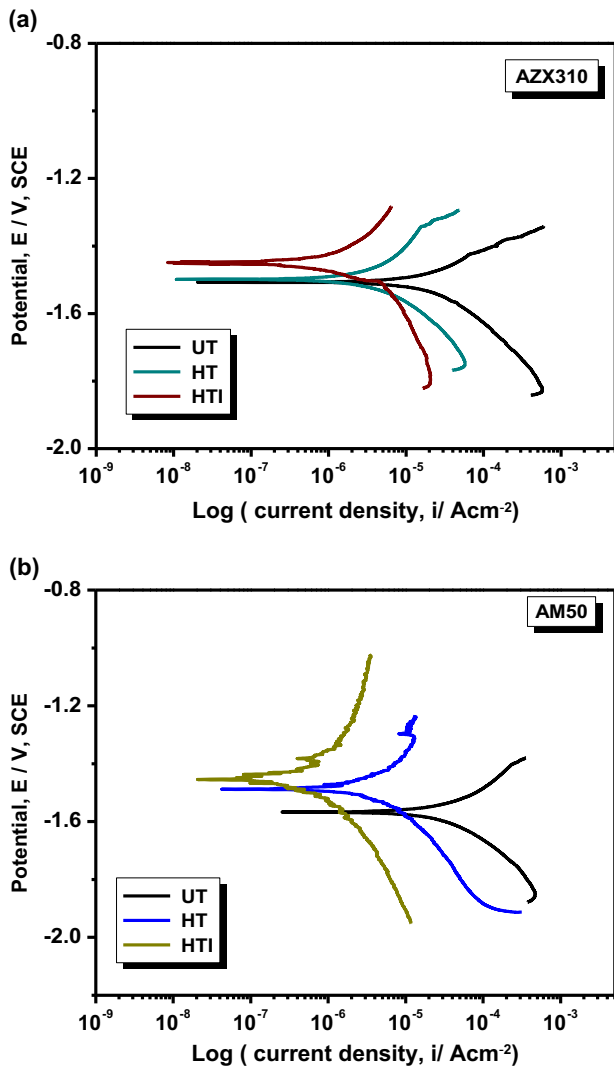
Fig. 8 Potentiodynamic polarization curves of **a** AZX310 and **b** AM50 alloys in SBF solution



Fig. 9 Electrochemical impedance spectra of AZX310 alloy in SBF solution

**Table 3** Electrochemical Tafel polarization parameters for AZX310 and AM50 Mg alloys in SBF solution

| Alloys | Treatment | $E_{corr}$ (V/ SCE) | $i_{corr}$ ($\mu$A/ cm$^2$) | $\beta a$ (mV/ decade) | $\beta c$ (mV/ decade) | Corrosion rate (mm/ year) |
|---|---|---|---|---|---|---|
| AZX310 | UT | −1.50 | 38.99 | 90 | 83 | 890.96 |
| | HT | −1.49 | 8.67 | 74 | 94 | 198.22 |
| | HTI | −1.44 | 1.62 | 91 | 82 | 37.14 |
| AM50 | UT | −1.56 | 36.88 | 84 | 78 | 842.73 |
| | HT | −1.47 | 5.16 | 75 | 69 | 118.11 |
| | HTI | −1.42 | 0.82 | 63 | 74 | 18.76 |

## 4.3 Electrochemical analysis

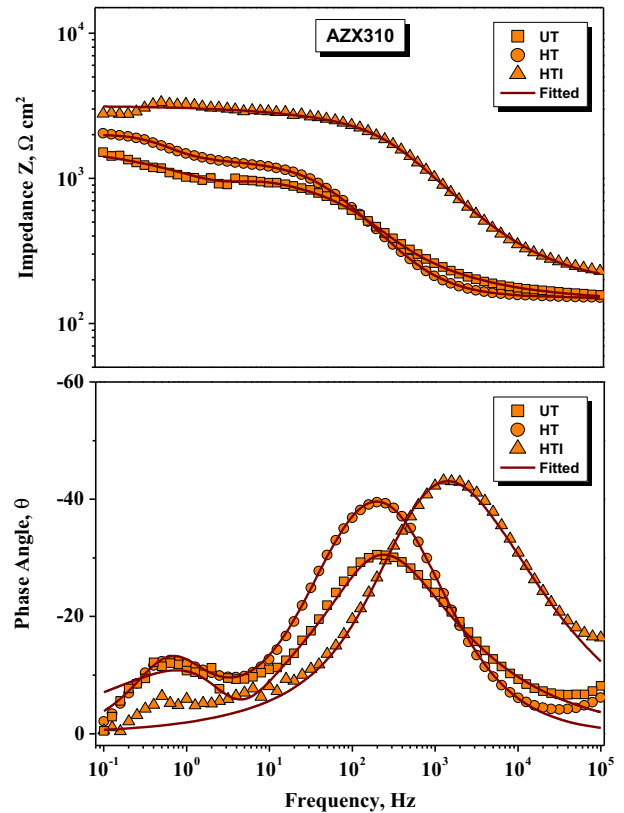From the polarization curves, the $E_{corr}$ values obtained for all the specimens were found to be in the range of potential from −1.42 to −1.56 V. The obtained corrosion potential $(E_{corr})$ values for UT AZX310 and AM50 specimens were about −1.50 and −1.56 V respectively. In contrast, the corrosion potentials of the HT AZX310 and AM50 specimens were shifted slightly towards on the positive shift to −1.49 and −1.47 V. Meanwhile for the HTI AZX310 and AM50 specimens, significant shift of potential towards the positive direction to −1.44 and −1.42 V was obtained which implies that HTI AZX310 and AM50 specimens possess higher corrosion potential than HT, UT AZX310 and AM50 specimens. Also the corrosion current density $(i_{corr})$ values obtained for UT AZX310 and AM50 alloys were 38.99 and 36.88 $\mu$A/cm$^2$ respectively. The HT AZX310 and AM50 specimens exhibited the values of 8.67 and 5.16 $\mu$A/ cm$^2$. In contrast, the HTI AZX310 and AM50 specimens represented the values of 1.62 and 0.82 $\mu$A/cm$^2$ respectively. It is a well known fact that high $E_{corr}$ and low $i_{corr}$ indicate a good anticorrosion property [44]. So, it can be obviously identified from the polarization curves that the HTI AM50 exhibited lower corrosion current $(i_{corr})$ value with two orders of magnitude with a lower corrosion rate value of 18.76 mm/ year was obtained when compared to other specimens. Hence, the polarization results showed that HTI AM50 exhibited higher corrosion resistance with lower corrosion current. From this, we can infer that during the longer time immersion
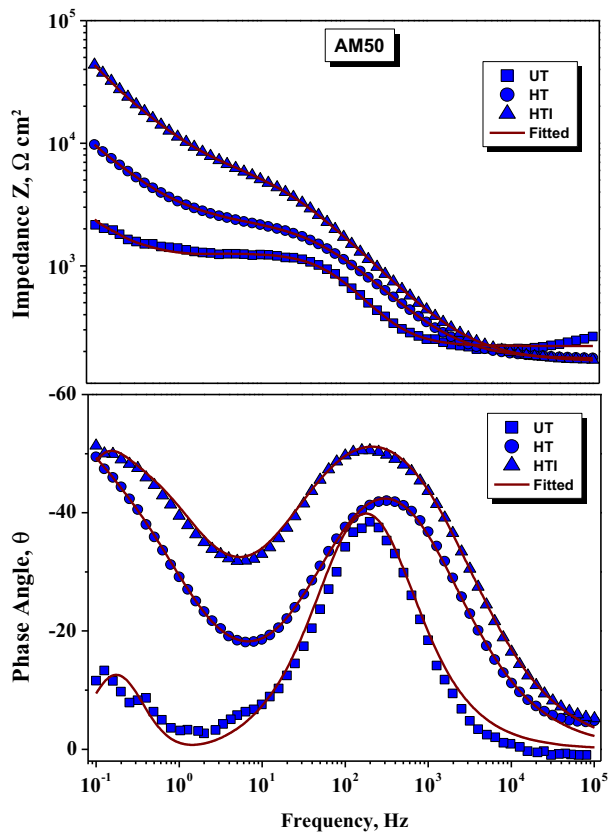
**Fig. 10** Electrochemical impedance spectra of AM50 alloy in SBF solution

**Table 4** Surface roughness values obtained for AZX310 and AM50 alloys

| Alloys | Surface treatment | Surface roughness $R_a$ (μm) |
|--------|-------------------|------------------------------|
| AZX310 | UT | −0.45 |
|        | HT | −0.88 |
|        | HTI | −1.35 |
| AM50   | UT | −0.52 |
|        | HT | −1.05 |
|        | HTI | −0.96 |

in SBF, the interaction of more Ca and P ions can absorb over the surface and forms a thick film of DCPD coating over HTI AM50 which enhances the corrosion protection over its surfaces and possess excellent corrosion resistance which is very essential for the bio-implant materials.

The electrochemical impedance response for the UT AZX310 (Fig. 9) and UT AM50 (Fig. 10) showed a single layer of a thin passive oxide film formation on the surfaces with insulative in nature. However, a small bump observed in the lower frequency region from $10^0$ to $10^{-1}$ Hz may be due to the formation of Mg(OH)$_2$ layer. The chloride ions from the SBF solution will transform the Mg(OH$_2$) film surface into soluble MgCl$_2$ in addition to the corrosion products. So

the surface will be more active due to the dissolution of Mg (OH$_2$) and there was a decrease in the protective surface area to promote for further dissolution of Mg [45].

The HT, HTI AZX310 (shown in Fig. 9) showed a duplex layer over its surface with inner oxide layer and outer DCPD coating layer formation and also after immersion in SBF (as evinced by XRD and ATR-IR analysis). Meanwhile for the HT, HTI AM50 (shown in Fig. 10) the spectra exhibited with duplex layers of two well defined distinct humps which are clearly visible at the higher and lower frequency regions. The distinct hump represents the two layers consists of inner oxide layer formation at high frequency and outer coating DCPD layer formation at lower frequency regions respectively [46]. The interaction of solution ions are identified generally by a phase angle shift at the high frequency region and a physical change of the DCPD layer at the low frequency region. Hence, it can be observed that the impedance response behavior for HTI AM50 was achieved significantly with greater enhancement of high corrosion resistance value compared with HTI, HT and UT AZX310.

EIS data obtained were been fitted and the fitting procedure establish a good deal with theoretical and experimental data by introducing a frequency dependent term as constant phase element (CPE) instead of using a pure capacitor. The electrochemical impedance response for the constant phase element (CPE) is given by

$$Z_{CPE} = [Q(jw)n]^{-1} \qquad (2)$$

where $Z$ represents the impedance, $Q$ is the Constant Phase Element (CPE), $\omega$ represents the angular frequency $= 2\sqrt{\Pi}f$ (rad s$^{-1}$), j denotes the imaginary number (j $= \sqrt{1}$), $n$ and $Q$ represents the frequency independent parameters depends on the temperature conditions. In general, the conditions applied for any electrochemical system will mainly depends on the value of $n$ which is given by $n$ is $-1 \le n \le 1$. When the value of when $n = 1$, it represents an ideal capacitor, and when $n = 0$, it denotes a pure resistor, and when $n = -1$, it represents a pure inductor. The appearance of CPE usually denoted by $Q$ an ideal capacitor was mainly introduced instead of a pure capacitor because of the presence of inhomogeneity at the surface of the electrode. It can also define in other terms by distribution of relaxation times which may arise due to the non-uniform diffusion of an inhomogeneous distribution of RC transmission line with an electrical analog. In the fitting method, a term chi-square value represents a good deal with the theoretical and experimental data values of using $Q$. The main criteria for the choosing the best fit of the EIS data model was to be the low chi-square values and with the low % error for the obtained parameters in the impedance spectrum.

**Table 5** Fitted Impedance parameters for AZX310 and AM50 alloys using $R_s(R_{ct}Q_{dl})$ $(R_fQ_f)$ model in SBF solution

| Alloys | Surface treatment | $R_s$ ($\Omega$ cm$^2$) | $R_f$ ($\Omega$ cm$^2$) | $Q_f$ ($\mu$F cm$^{-2}$) | $n$ | $R_{ct}$ ($\Omega$ cm$^2$) | $Q_{dl}$ ($\mu$F cm$^{-2}$) | $n$ |
|---|---|---|---|---|---|---|---|---|
| AZX310 | UT | 52.50 | 1556 | 58.91 | 0.91 | – | – | – |
| | HT | 43.24 | 2048 | 39.14 | 0.93 | 1081 | 59.24 | 0.94 |
| | HTI | 41.97 | 3126 | 3.59 | 0.94 | 2758 | 19.54 | 0.92 |
| AM50 | UT | 53.99 | 2115 | 22.82 | 0.95 | – | – | – |
| | HT | 46.21 | 9933 | 2.59 | 0.96 | 2084 | 22.25 | 0.95 |
| | HTI | 47.82 | 43560 | 1.27 | 0.96 | 4369 | 9.64 | 0.94 |
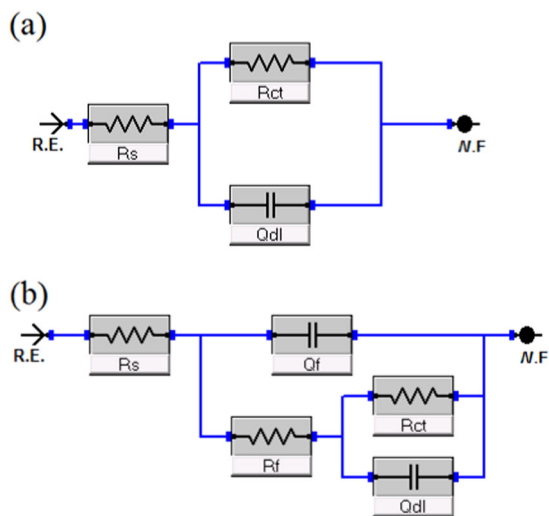


**Fig. 11** Equivalent circuit diagrams fitted for AZX310 and AM50 alloys in SBF solution **a** UT, **b** HT, HTI

The equivalent electrical circuit model fitted for the UT AZX310 and UT AM50 alloys was $R_s(R_{ct}Q_{dl})$ presented in (Fig. 11a) which represents the single passive layer formation on the surface of the specimens. The equivalent electrical circuit model fitted for HT, HTI AZX310 and AM50 alloys was $R_s(R_{ct}Q_{dl})$ $(R_fQ_f)$ shown in (Fig. 11b). Here, the term $R_s$ denotes the solution resistance of the electrolyte solution, $R_{ct}$ and $R_f$ parameters correspond to the charge transfer resistance of the oxide layer and the coating layers, respectively. $Q_{dl}$ and $Q_f$ parameters correspond to the double layer capacitance of the oxide layer and the DCPD coating layer formation on the surface of AZX310 and AM50 alloys.

Electrochemical impedance values derived from the impedance plots and the fitted impedance values were given in Table 5. It can be observed that, the initial increase in the $R_b$ value represents the passive film thickness and the change in the passive film behavior which accounts for better corrosion protection. This represents that the corrosion of Mg surfaces are prohibited mainly due to the inner oxide layer and facilitates the growth of oxide layer for the UT AZX310 and AM50 alloys. In the case of HT, HTI AZX310 and AM50 alloys, it can be identified that the $R_f$

values are very high compared to $R_{ct}$ values which indicated the impedance response is more dominant for the newly formed DCPD coating layer. However, the HTI AM50 exhibited with higher corrosion resistance value ($R_f$) compared with the other specimens which indicated the thick DCPD layer formation with more CaP deposition after the immersion in SBF [45, 46].

## 5 Conclusions

DCPD brushite coating with flake like crystal structure was prepared through chemical deposition treatment for AZX310 and AM50 alloys for the corrosion protection ability and enhancement of biocompatibility. *In vitro* characterization studies exhibited the DCPD coating formation with CaP (calcium phosphate) layer over the surfaces of HT and HTI AZX310 and AM50 alloys. DCPD coating formation of CaP layer was confirmed using SEM, EDS, AFM, XRD and ATR-IR characterization studies. The hydrophilicity of the DCPD coatings was evaluated using water contact angle measurements. Electrochemical characterization of polarization and impedance spectroscopic studies revealed that HTI AM50 exhibited with higher corrosion resistance and lower corrosion current density compared with other specimens. Among the surface treated AZX310 and AM50 alloys, the surface of HTI AM50 is more favourable with DCPD formation of more CaP deposition which induces excellent biocompatibility, super hydrophilicity nature and excellent corrosion performance within a short period of time essentially required for the Osseointegration of orthopaedic bio-implants.

## Compliance with ethical standards

**Conflict of interest** The authors declare that they have no conflict of interest.

# References

1. Xin Y, Hu T, Chu PK. In vitro studies of biomedical magnesium alloys in a simulated physiological environment: a review. Acta Biomater. 2011;7:1452–9.

2. Kannan MB, Raman RK. In vitro degradation and mechanical integrity of calcium-containing magnesium alloys in modified-simulated body fluid. Biomaterials. 2008;29:2306–14.

3. Li Y, Wen C, Mushahary D, Sravanthi R, Harishankar N, Pande G, Hodgson P. Mg-Zr-Sr alloys as biodegradable implant materials. Acta Biomater. 2012;8:3177–88.

4. Staiger MP, Pietak AM, Huadmai J, Dias G. Magnesium and its alloys as orthopedic biomaterials: a review. Biomaterials. 2006;27:1728–34.

5. Saris NEL. Magnesium: an update on physiological, clinical and analytical aspects. Clin Chim Acta. 2000;294:1–26.

6. Song GL. Control of biodegradation of biocompatable magnesium alloys. Corros Sci. 2007;49:1696–701.

7. Witte F, Ulrich H, Rudert M, Willbold E. Biodegradable magnesium scaffolds: part I: appropriate inflammatory response. J Biomed Mater Res Part A. 2007;81:748–65.

8. Gérrard Eddy JP, Sridevi B, Derek F. Biomedical magnesium alloys: a review of material properties, surface modifications and potential as a biodegradable orthopaedic implant. Am J Biomed Eng. 2012;2:218–40.

9. Regine W, Anneke M, Frank F. Optimization of cell adhesion on Mg based implant materials by pre-Incubation under cell culture conditions. Int J Mol Sci. 2014;15:7639–50.

10. Pietrzak WS. Principles of development and use of absorbable internal fixation. Tissue Eng. 2000;6:25–433.

11. Gray-Munro JE, Strong M. The mechanism of deposition of calcium phosphate coatings from solution onto magnesium alloy AZ31. J Biomed Mater Res A. 2009;90:339–50.

12. Gray-Munro JE, Seguin C, Strong M. Influence of surface modification on the in vitro corrosion rate of magnesium alloy AZ31. J Biomed Mater Res A. 2009;91:221–30.

13. Tomozawa M, Hiromoto S. Microstructure of hydroxyapatite and octacalcium phosphate-coatings formed on magnesium by a hydrothermal treatment at various pH values. Acta Mater. 2011;59:355–63.

14. Chen XB, Birbilis N, Abbott TB. Review of corrosion-resistant conversion coatings for magnesium and its alloys. Corros Sci. 2011;53:2263–8.

15. Wang HX, Guan SK, Wang X, Ren CX, Wang LG. In vitro degradation and mechanical integrity of Mg-Zn-Ca alloy coated with Ca-deficient hydroxyapatite by the pulse electrodeposition process. Acta Biomater. 2010;6:1743–8.

16. Song YW, Shan DY, Han EH. Electrodeposition of hydroxyapatite coating on AZ91D magnesium alloy for biomaterial application. Mater Lett. 2008;62:3276–9.

17. Jamesh M, Kumar S, Sankara Narayanan T. Electrodeposition of hydroxyapatite coating on magnesium for biomedical applications. J Coat Technol Res. 2012;9:495–502.

18. Wen C, Guan S, Peng L, Ren C, Wang X, Hu Z. Characterization and degradation behavior of AZ31 alloy surface modified by bone-like hydroxyapatite for implant applications. Appl Surf Sci. 2009;255:6433–8.

19. Dorozhkin SV. Calcium orthophosphate coatings on magnesium and its biodegradable alloys. Acta Biomater. 2014;10:2919–34.

20. Shadanbaz S, Dias GJ. Calcium phosphate coatings on magnesium alloys for biomedical applications: a review. Acta Biomater. 2012;8:20–30.

21. Surmenev RA, Surmeneva MA, Ivanova AA. Significance of calcium phosphate coatings for the enhancement of new bone osteogenesis—a review. Acta Biomater. 2014;10:557–79.

22. Paital SR, Dahotre NB. Calcium phosphate coatings for bio-implant applications: materials, performance factors, and methodologies. Mater Sci Eng R. 2009;66:1–70.

23. Burg KJL, Porter S, Kellam JF. Biomaterial developments for bone tissue engineering. Biomaterials. 2000;21:2347–59.

24. Müller WD, Nascimento ML, Zeddiese M, Córsico M, Gassa LM, Lorenzo MAF. de Mele, magnesium and its alloys as degradable biomaterials: corrosion studies using potentiodynamic and EIS electrochemical techniques. Mater Res. 2007;10:5–10.

25. Chen Y, Miao X. Effect of fluorine addition on the corrosion resistance of hydroxyapatite ceramics. Ceram Int. 2004;30:1961–5.

26. Gopi D, Bhalaji PR, Ramya S, Kavitha L. Evaluation of biodegradability of surface treated AZ91 magnesium alloy in SBF solution. J Ind Eng Chem. 2015;23:218–27.

27. Hiromoto S, Tomozawa M. Hydroxyapatite coating of AZ31 magnesium alloy by a solution treatment and its corrosion behavior in NaCl solution. Surf Coat Technol. 2011;205:4711–9.

28. Zucchi F, Grassi V, Furigana A, Monticelli C, Trabanelli G. Electrochemical behaviour of a magnesium alloy containing rare earth elements. J Appl Electrochem. 2006;36:195–204.

29. Li L, Gao J, Wang Y. Evaluation of cyto-toxicity and corrosion behavior of alkali-heat-treated magnesium in simulated body fluid. Surf Coat Technol. 2004;185:92–98.

30. Zhu Y, Wu G, Zhang YH, Zhao Q. Growth and characterization of $Mg(OH)_2$ film on magnesium alloy AZ31. Appl Surf Sci. 2011;257:6129–37.

31. Lorenz C, Brunner JG, Kollmannsberger P, Jaafar L, Fabry B, Virtanen S. Effect of surface pre-treatments on biocompatibility of magnesium. Acta Biomater. 2009;5:2783–9.

32. Zhao H, Cai S, Niu S, Zhang R, Wu X, Xu G, Ding Z. The influence of alkali pretreatments of AZ31 magnesium alloys on bonding of bioglass–ceramic coatings and corrosion resistance for biomedical applications. Ceram Int. 2015;41:4590–600.

33. Su Y, Lu Y, Su Y, Hu J, Lian J, Li G. Enhancing the corrosion resistance and surface bioactivity of a calcium-phosphate coating on a biodegradable AZ60 magnesium alloy via a simple fluorine post-treatment method. RSC Adv. 2015;5:56001–10.

34. Su Y, Li G, Lian JA. Chemical conversion hydroxyapatite coating on AZ60 magnesium alloy and its electrochemical corrosion behaviour. Int J Electrochem Sci. 2012;7:11497–511.

35. Ou C, Lu W, Zhan Z, Huang P, Yan P, Yan B, Chen M. Effect of Ca and P ion concentrations on the structural and corrosion properties of biomimetic Ca-P coatings on ZK60 magnesium alloy. Int J Electrochem Sci. 2013;8:9518–30.

36. Kokubo T, Takadama H. How useful is SBF in predicting in vivo bone bioactivity. Biomaterials. 2005;27:2907–15.

37. Wang Y, Wei M, Gao J. Improve corrosion resistance of magnesium in simulated body fluid by dicalcium phosphate dihydrate coating. Mater Sci Eng C. 2009;29:1311–6.

38. Sridevi B, Gérrard Eddy JP, Derek F. Growth of flower-like brushite structures on magnesium substrates and their subsequent low temperature transformation to hydroxyapatite. Am J Biomed Eng. 2014;4:79–87.

39. Wen C, Guan S, Peng L, Ren C, Wang X, Hu Z. Characterization and degradation behavior of AZ31 alloy surface modified by bone-like hydroxyapatite for implant applications. Appl Surf Sci. 2009;255:6433–8.

40. Dorozhkin SV. A review on the dissolution of calcium apatites. Prog Cryst Growth Charact. 2002;44:45–61.

41. Mukhametkaliyev TM, Surmeneva MA, Vladescu A, Cotruta CM, Braic M, Dinu M, Vranceanu MD, Pana I, Muellere M, Surmenev RA. A biodegradable AZ91 magnesium alloy coated with a thin nanostructured hydroxyapatite for improving the corrosion resistance. Mater Sci Eng C. 2017;75:95–103.

42. Zhao Y-B, Liu H-P, Li C-Y, Chen Y, Li S-Q, Zeng R-C, Wang Z-L. Corrosion resistance and adhesion strength of a spin-assisted layer-by-layer assembled coating on AZ31 magnesium alloy. Appl Surf Sci. 2018;434:787–95.

43. Sasikumar Y, Solomon MM, Olasunkanmi LO, Ebenso EE. Effect of surface treatment on the bioactivity and electrochemical behavior of magnesium alloys in simulated body fluid. Mater Corros. 2017;68:776–90.

44. Zhang YJ, Yan CW, Wang FH, Li WF. Electrochemical behavior of anodized Mg alloy AZ91D in chloride containing aqueous solution. Corros Sci. 2005;47:2816–31.

45. Chen C, Qiu S, Qin S, Yan G, Zhao H, Wang L. Anticorrosion performance of epoxy coating containing reactive poly (o-phenylenediamine) nanoparticles. Int J Electrochem Sci. 2017;12:3417–31.

46. Sasikumar Y, Rajendran N. Influence of surface modification on the apatite formation and corrosion behavior of Ti and Ti–15Mo alloy for biomedical applications. Mater Chem Phys. 2013;138:114–23.